Modeling nuclei of radio galaxies from VLBI radio observations. Application to the BL Lac Object S5 1803+784

J. Roland, S. Britzen, N. A. Kudryavtseva, A. Witzel, M. Karouzos

A&A 483, 125–135 (2008)
DOI: 10.1051/0004-6361:20078521

Astronomy & Astrophysics

Modeling nuclei of radio galaxies from VLBI radio observations

Application to the BL Lac Object S5 1803+784

J. Roland[1], S. Britzen[2], N. A. Kudryavtseva[2,3,⋆], A. Witzel[2], and M. Karouzos[2]

[1] Institut d'Astrophysique, UPMC Univ Paris 06, CNRS, UMR 7095, 98 bis Bd Arago, 75014 Paris, France
e-mail: roland@iap.fr
[2] Max-Planck-Institut für Radioastronomie, Auf dem Hügel 69, Bonn 53121, Germany
[3] Astronomical Institute of St.-Petersburg State University, Petrodvorets, Universitetsky pr. 28, 198504 St.-Petersburg, Russia

Received 21 August 2007 / Accepted 15 February 2008

ABSTRACT

We present a new method to fit the variations of both coordinates of a VLBI component as a function of time, assuming that the nucleus of the radio source contains a binary black hole system (BBH system). The presence of a BBH system produces 2 perturbations of the trajectory of the ejected VLBI components. By using only the VLBI coordinates, the problem we have to solve reduces to an astrometric problem. Knowledge of the variations of the VLBI coordinates as a function of time contains the kinematical information, thus we are able to deduce the inclination angle of the source and the bulk Lorentz factor of the ejected component. Generally, there is a family of the BBH system producing the same fit to our data. To illustrate this method, we apply it to the source 1807+784. We find that the inclination of the source is $i_o = 5.8° \, ^{+1.7}_{-1.8}$ and the VLBI component is ejected with a bulk Lorentz factor of $\gamma = 3.7 \, ^{+0.3}_{-0.2}$. We determine the family of the BBH system which provides the best fit, assuming at first that the masses of the 2 black holes are equal and then that the masses are different. Each family of BBH systems is characterized by $T_p/T_b \approx 1.967$, where T_p and T_b are the precession period of the accretion disk of the black hole ejecting the VLBI component and the orbiting period of the BBH system.

Key words. astrometry – galaxies: BL Lacertae objects: individual: 1803+784 – galaxies: jets

1. Introduction

In previous articles, (Britzen et al. 2001; Lobanov & Roland 2005) we have shown that VLBI and optical observations of compact radio sources can be explained if their nuclei contain a binary black hole system (BBH system). However, for most of the compact radio sources we have only VLBI observations.

In this article we present a method to fit the VLBI observations using a BBH system.

This method requires knowledge of the variations of the two coordinates of the VLBI component as a function of time. As these observations contain the kinematical information needed, we are able to deduce the inclination angle of the source and the bulk Lorentz factor of the ejected component.

We propose a geometric model that assumes that the motion of a component ejected by the nucleus of the radio source is perturbed by two different motions, namely:

1. the precession of the accretion disk;
2. the motion of the two black holes around the gravity center of the BBH system.

In addition to these two perturbations, the ejected flow is perturbed by the slow motion of the BBH system around the center of gravity of the galaxy. This third perturbation is often observed in compact radio sources and is responsible for the slow bending of the VLBI jet, i.e., the mean ejection direction changes slowly as the distance of the component from the core increases. This bending becomes prominent at a distance from the core of a few milliarcsecond (mas). Thus, by studying the motion of the VLBI component in the innermost part of the VLBI jet, we can expect that the influence of the slow motion of the BBH system is negligible compared to the perturbations induced by the precession of the accretion disk and the motion of the black holes around the gravity center of the BBH system. The inclusion of this slow motion in this model would be difficult as the characteristics of the BBH system motion around the gravity center of the galaxy (i.e. the radius, the speed) are essentially unknown.

According to the above, in order to model the ejection of VLBI components by a BBH system, observations of a component moving in the first mas of the VLBI jet are needed. Using just the VLBI coordinates and a geometric model, the problem we have to solve reduces to an astrometric one.

The method presented in Lobanov & Roland (2005) was not consistent. In this article we built a consistent method that solves the problems found in Lobanov & Roland (2005).

In Sect. 2 we will present the details of the model and in Sect. 3 the new method.

To illustrate the method, we apply it to the source S5 1803+784 and we show how, from the knowledge of the variations of the coordinates $X(t)$ and $Y(t)$ of a VLBI component, we can derive

- the inclination angle of the source;
- the bulk Lorentz factor of the ejected component;
- the angle between the accretion disk and the plane of the BBH system;
- the size of the BBH system;

⋆ Member of the International Max Planck Research School (IMPRS) for Radio and Infrared Astronomy at the Universities of Bonn and Cologne.

– the ratio T_p/T_b, where T_p is the precession period of the accretion disk and T_b the orbiting period of the BBH system;
– the origin of the ejection of the VLBI component;
– the duration of the ejection of the plasma responsible for the VLBI component.

2. The model

2.1. Introduction: the two-fluid model

We will describe the ejection of a VLBI component in the framework of the two-fluid model (Sol et al. 1989; Pelletier & Roland 1989, 1990; Pelletier & Sol 1992). The two-fluid description of the outflow is adopted with the following assumptions:

1. the outflow consists of an $e^- - p$ plasma (hereafter *the jet*) moving at mildly relativistic speed $v_j \leq 0.4 \times c$ and an $e^\pm$ plasma (hereafter *the beam*) moving at highly relativistic speed (with corresponding Lorentz factor $\gamma_b \leq 30$);
2. the magnetic field lines are parallel to the flow in the beam and the mixing layer, and are toroidal in the jet (see Fig. 1 of Lobanov & Roland 2005).

The $e^- - p$ jet carries most of the mass and the kinetic energy ejected by the nucleus. It is responsible for the formation of kpc-jets, hot spots and extended lobes (Muxlow et al. 1988; Roland et al. 1988; Roland & Hetem 1996). The relativistic $e^\pm$ beam moves in a channel through the mildly relativistic jet and is responsible for the formation of superluminal sources and their γ-ray emission (Roland et al. 1994). The relativistic beam can propagate if the magnetic field B is parallel to the flow in the beam and in the mixing layer between the beam and the jet and if it is greater than a critical value (Pelletier et al. 1988; Achatz & Schlickeiser 1993). The magnetic field in the jet becomes rapidly toroidal (Pelletier & Roland 1990).

The observational evidence for the two-fluid model has been discussed by e.g. Roland & Hetem (1996). Recent observational evidence for relativistic ejection of an $e^\pm$ beam come from the γ-ray observations of MeV sources (Roland & Hermsen 1995; Skibo et al. 1997) and from VLBI polarization observations (Attridge et al. 1999).

The formation of X-ray and γ-ray spectra, assuming relativistic ejection of $e^\pm$ beams, has been investigated by Marcowith et al. (1995, 1998) in the case of Centaurus A.

The possible existence of VLBI components with two different speeds has been recently pointed out in the case of the radio galaxies Centaurus A (Tingay et al. 1998), Virgo A (Biretta et al. 1999) and 3C 120 (Gomez et al. 2001). If the relativistic beam transfers some energy and/or relativistic particles to the jet, the relativistic particles in the jet will radiate and a new VLBI component with a mildly relativistic speed will be observed (3C 120 is a good example of a source showing this effect).

2.2. The geometry of the model

We will call Ω the angle between the accretion disk and the orbital plane (XOY) of the BBH system. The ejection of the component will be on a cone with its axis in the $Z'OZ$ direction and opening angle Ω. We will assume that the line of sight is in the plane (YOZ) and forms an angle i_o with the axis $Z'OZ$ (see Fig. 1). The plane perpendicular to the line of sight is the plane (ηOX). We will call $\Delta\Xi$ the angle of the rotation in the plane perpendicular to the line of sight, in order to transform the coordinates η and X into coordinates N (North) and W (West), which are directly comparable with the VLBI observations. We have

$$W = x\cos(\Delta\Xi) - (z\sin(i_o) + y\cos(i_o))\sin(\Delta\Xi), \quad (1)$$

$$N = x\sin(\Delta\Xi) + (z\sin(i_o) + y\cos(i_o))\cos(\Delta\Xi). \quad (2)$$

2.3. The precession model

Here we describe the precession of the accretion disk.

The coordinates of a component moving in the perturbed beam are given by

$$x_c = R_o(z)\cos(\omega_p t - k_p z(t) + \phi_o), \quad (3)$$

$$y_c = R_o(z)\sin(\omega_p t - k_p z(t) + \phi_o), \quad (4)$$

$$z_c = z_c(t), \quad (5)$$

where $\omega_p = 2\pi/T_p$, T_p is the precession period, and k_p is defined by

$$k_p = 2\pi/T_p V_a, \quad (6)$$

where V_a is the speed of the propagation of the perturbations and a free parameter of the problem.

We will assume that the amplitude of the perturbation first increases linearly, and we take the form of the amplitude $R(z_c(t))$ to be

$$R(z_c(t)) = \frac{R_o z_c(t)}{(a + z_c(t))}, \quad (7)$$

where a is

$$a = R_o/(2\ \tan\Omega). \quad (8)$$

2.4. The binary system model

To explain the origin of the precession of the accretion disk, we propose that the nucleus hosts a BBH system.

As stated above, the two black holes orbit in the plane (XOY), and the origin of our coordinate system is centered on the mass center of the system. The elliptical orbit is given by

$$r = \frac{p}{1 + e\ \cos(\varphi)}, \quad (9)$$

where e and p are respectively the eccentricity and the parameter or the semi-latus rectum of the orbit.

We will assume that the two black holes have circular orbits, i.e. $e = 0$ and we will define the black hole that ejects the VLBI component with index 1. Its coordinates are:

$$X_1(t) = -\frac{M_2}{M_1 + M_2} p\cos(\psi(t)), \quad (10)$$

$$Y_1(t) = -\frac{M_2}{M_1 + M_2} p\sin(\psi(t)). \quad (11)$$

As the orbits are circular, we have $\psi(t) = \omega_b t + \psi_o$. Writing

$$x_1 = y_1 = -\frac{pM_2}{M_1 + M_2}, \quad (12)$$

we have

$$x_1 = -\frac{M_2}{M_1 + M_2} \times \left[\frac{T_b^2}{4\pi^2} G(M_1 + M_2)\right]^{1/3}, \quad (13)$$

where T_b is the period of the BBH system.

We define $R_{\rm bbh}$ the distance between the two black holes as the size of the BBH system, it is:

$$R_{\rm bbh} = \left[\frac{T_{\rm b}^2}{4\pi^2} G(M_1 + M_2)\right]^{1/3}. \quad (14)$$

The coordinates of black hole 1 can be written

$$X_1(t) = x_1 \cos(\omega_{\rm b} t + \psi_{\rm o}), \quad (15)$$

$$Y_1(t) = y_1 \sin(\omega_{\rm b} t + \psi_{\rm o}). \quad (16)$$

Finally, we suppose that the perturbation of the beam is damped with a characteristic time $T_{\rm d}$.

For VLBI observations the origin of the coordinates is black hole 1, i.e. the black hole ejecting the VLBI components. Therefore, the coordinates of the moving components *in the frame of reference where black hole 1 is considered the origin* are

$$\begin{aligned} x_{\rm c} &= [R_{\rm o}(z)\cos(\omega_{\rm p} t - k_{\rm p} z(t) + \phi_{\rm o}) \\ &\quad + x_1 cos(\omega_{\rm b} t - k_{\rm b} z(t) + \psi_{\rm o}) - x_1 \cos(\psi_{\rm o})] \\ &\quad \times \exp(-t/T_{\rm d}), \end{aligned} \quad (17)$$

$$\begin{aligned} y_{\rm c} &= [R_{\rm o}(z)\sin(\omega_{\rm p} t - k_{\rm p} z(t) + \phi_{\rm o}) \\ &\quad + y_1 \sin(\omega_{\rm b} t - k_{\rm b} z(t) + \psi_{\rm o}) - y_1 \sin(\psi_{\rm o})] \\ &\quad \times \exp(-t/T_{\rm d}), \end{aligned} \quad (18)$$

$$z_{\rm c} = z_{\rm c}(t), \quad (19)$$

where $\omega_{\rm b} = 2\pi/T_{\rm b}$, and $k_{\rm b}$ is defined by

$$k_{\rm b} = \frac{2\pi}{T_{\rm b} V_{\rm a}}. \quad (20)$$

The differential equation governing the evolution of $z_{\rm c}(t)$ can be obtained through the relation for the speed of the component

$$v_{\rm c}^2 = \left(\frac{{\rm d}x_{\rm c}(t)}{{\rm d}t}\right)^2 + \left(\frac{{\rm d}y_{\rm c}(t)}{{\rm d}t}\right)^2 + \left(\frac{{\rm d}z_{\rm c}(t)}{{\rm d}t}\right)^2, \quad (21)$$

where $v_{\rm c}$ is related to the bulk Lorentz factor by $v_{\rm c}/c = \sqrt{(1 - 1/\gamma_{\rm c}^2)}$.

Using (3), (4) and (5), we find from (21) that ${\rm d}z_c/{\rm d}t$ is the solution of the equation

$$A\left(\frac{{\rm d}z_{\rm c}}{{\rm d}t}\right)^2 + B\left(\frac{{\rm d}z_{\rm c}}{{\rm d}t}\right) + C = 0. \quad (22)$$

A calculation of the coefficients A, B and C can be found in Appendix A.

Equation (22) admits two solutions corresponding to the jet and the counter-jet.

We assumed that the line of sight is in the plane (YOZ) and makes an angle $i_{\rm o}$ with the z axis (see Fig. 1). Thus following Camenzind & Krockenberger (1992), if we call θ the angle between the velocity of the component and the line of sight we have

$$\cos(\theta(t)) = \left(\frac{{\rm d}y_{\rm c}}{{\rm d}t}\sin\, i_{\rm o} + \frac{{\rm d}z_{\rm c}}{{\rm d}t}\cos\, i_{\rm o}\right)/v_{\rm c}. \quad (23)$$

The Doppler beaming factor δ, characterizing the anisotropic emission of the moving component, is

$$\delta_{\rm c}(t) = \frac{1}{\gamma_{\rm c}\,[1 - \beta_{\rm c}\cos(\theta(t))]}, \quad (24)$$

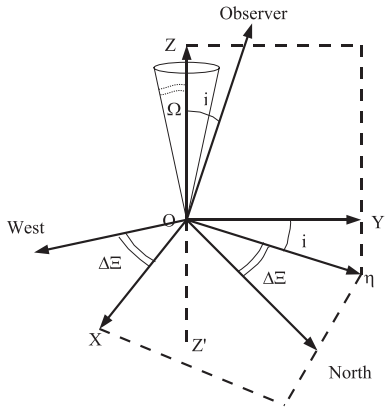

Fig. 1. The geometry of the problem.

where $\beta_{\rm c} = v_{\rm c}/c$. The observed flux density is

$$S_{\rm c} = \frac{1}{D^2}\delta_{\rm c}(t)^{2+\alpha_r}(1+z)^{1-\alpha_r}\int_{\rm c} j_{\rm c}{\rm d}V, \quad (25)$$

where D is the luminosity distance of the source, z its redshift, $j_{\rm c}$ is the emissivity of the component, and $\alpha_{\rm r}$ is the synchrotron spectral index (a negative definition of the spectral index, $S \propto \nu^{-\alpha}$ is used). As the component is moving relativistically toward the observer, the observed time is shortened and is given by

$$t_{\rm obs} = \int_0^t [1 - \beta_{\rm c}\cos(\theta(t'))]\,(1+z)\,{\rm d}t'. \quad (26)$$

3. The global method

3.1. Introduction

In Lobanov & Roland (2005) we provide a method to determine the characteristic parameters of the BBH system using radio and optical observations. The method consists of two steps, i.e. in a first step we use VLBI observations to model the precession (without a BBH system) and in a second step we use optical observations to obtain the characteristic parameters of the BBH system.

The above described method has the following problems:

1. using a simple precession model, we find for 3C 345 that a bulk Lorentz factor increasing with time is necessary.
2. *using the parameters of the precession found in the first step,* the BBH solution obtained in the second step is not necessarily consistent with the precession solution found previously. Indeed, in the limit $M_2 \to 0$ the BBH solution is not necessarily able to reproduce the results of the precession model found in the first step. The limit $M_2 \to 0$ corresponds to a single black hole and the precession of the accretion disk is due to the Lens-Thirring effect in that case.

The above problems can be solved if we directly model the VLBI observations with a BBH system instead of a simple precession model. In the BBH system model, the bulk Lorentz factor is constant, and the model explains the apparent variations of the speed of the VLBI component when it escapes from the nucleus (see Fig. 8; the apparent speed of the ejected component changes by a factor of four with a constant bulk Lorentz factor and it is not necessary to involve any acceleration or deceleration of the VLBI component). Since the BBH system and the precession solution are obtained simultaneously, they are obviously self-consistent.

We call the method we present in this article the global method.

In the global method, we calculate the projected trajectory on the plane of the sky of a component ejected by a BBH system and we determine the parameters of the model to simultaneously produce the best fit for both the West and North coordinates, i.e. $W_c(t)$, $N_c(t)$. So, the parameters found are such that minimize

$$\chi^2_t = \chi^2(W_c(t)) + \chi^2(N_c(t)), \tag{27}$$

where $\chi^2(W_c(t))$ and $\chi^2(N_c(t))$ are the χ^2 calculated by comparing the VLBI observations with the calculated coordinates $W_c(t)$ and $N_c(t)$ of the component.

3.2. The coordinates of the VLBI component

Solving (22), we determine the coordinate $z_c(t)$ of a point source component ejected relativistically in the perturbed beam. Then, using (17) and (18), we can find the coordinates $x_c(t)$ and $y_c(t)$ of the component. In addition, for each point of the trajectory, we can calculate the derivatives dx_c/dt, dy_c/dt, dz_c/dt and then deduce $\cos\theta$ from (23), δ_c from (24), S_ν from (25) and t_{obs} from (26).

When the coordinates $x_c(t)$, $y_c(t)$ and $z_c(t)$ have been calculated, they can be transformed to $w_c(t)$ (West) and $n_c(t)$ (North) coordinates using (1) and (2).

As explained in Britzen et al. (2001) and Lobanov & Roland (2005), the radio VLBI component has to be described as an extended component along the beam. Let us call n_{rad} the number of points (or steps along the beam) for which we integrate, in order to model the component. The coordinates $W_c(t)$, $N_c(t)$ of the VLBI component are then

$$W_c(t) = \left(\sum_{i=1}^{n_{rad}} w_{ci}(t)\right)/n_{rad}, \tag{28}$$

$$N_c(t) = \left(\sum_{i=1}^{n_{rad}} n_{ci}(t)\right)/n_{rad}. \tag{29}$$

and can be compared with the observed coordinates of the VLBI component.

3.3. The parameters of the model

In this section, we list what a priori the free parameters of the model are:

- i_o the inclination angle;
- ϕ_o the phase of the precession at $t = 0$;
- $\Delta\Xi$ the rotation angle in the plane perpendicular to the line of sight (see (1) and (2));
- Ω the opening angle of the precession cone (see (8));
- R_o the maximum amplitude of the perturbation (see (7));
- T_p the precession period of the accretion disk;
- T_d the characteristic time for the damping of the beam perturbation;
- M_1 the mass of the black hole ejecting the radio jet;
- M_2 the mass of the secondary black hole;
- γ_c the bulk Lorentz factor of the VLBI component;
- ψ_o the phase of the BBH system at $t = 0$;
- T_b the period of the BBH system;
- t_o the origin of the ejection of the VLBI component;
- V_a the propagation speed of the perturbations;
- n_{rad} is the number of steps to describe the extension of the VLBI component along the beam.

To begin with, we assume that $M_1 = M_2$ and when the corresponding solution is obtained, we calculate the family $M_1(M_2)$ which provides the same fit.

So, the problem we have to solve is a 14 free parameters problem.

If, in addition to the radio, optical observations are available that peak in the light curve, this optical emission can be modelled as the synchrotron emission of a point source ejected in the perturbed beam (Britzen et al. 2001; and Lobanov & Roland 2005). This short burst of very energetic relativistic $e^\pm$ is followed immediately by a very long burst of less energetic relativistic $e^\pm$. This long burst is modelled as an extended structure along the beam and is responsible for the VLBI radio emission. In that case the origin t_o of the VLBI component is the beginning of the first peak of the optical light curve and is not a free parameter of the model.

We have to investigate the different possible scenarios with regard to the sense of the rotation of the accretion disk and the sense of the orbital rotation of the BBH system. These possibilities correspond to $\pm\omega_p(t - z/V_a)$ and $\pm\omega_b(t - z/V_a)$. As the sense of the precession is always opposite to the sense of the orbital motion, we will study the two cases denoted by $+-$ and $-+$ where we have $\omega_p(t - z/V_a)$, $-\omega_b(t - z/V_a)$ and $-\omega_p(t - z/V_a)$, $\omega_b(t - z/V_a)$ respectively.

3.4. The method to solve the problem

To find a solution for the above described problem we use the following method.

As mentioned before we start with the assumption that $M_1 = M_2$, i.e. that the two masses of the BBH system are equal.

First, we find the inclination angle that provides the best fit. To do that we minimize $\chi^2_t(i_o)$ (see (27)) when the inclination angle varies gradually between two values. At each step of i_o, we determine each free parameter λ such that $\partial\chi^2_t/\partial\lambda = 0$ and χ^2_t presents a minimum.

Furthermore, using the inclination angle determined previously, we explore the space of the solutions, for a varying mass of the BBH system (while still assuming $M_1 = M_2$). This allow us to find whether the solution of the BBH system presents a degeneration or if there are other solutions, with different masses, that fit the observations. When exploring the solutions space, we always vary one parameter in a step-wise manner, with each step minimizing χ^2_t for each of the free parameters.

The space of the solutions can be explored for each of the free parameters if necessary.

Because the problem is a non-linear one, we calculate again the variations of $\chi^2_t(i_o)$ for the best solution found previously, starting from the inclination angle obtained in the first step. Where $\chi^2_t(i_o)$ reaches its minimum, we have

$$\left(\frac{\partial\chi^2}{\partial i_o}\right)_{min} = A\,(i_o - i_{o,min}), \tag{30}$$

and the 1σ error bar, $(\Delta i_o)_{1\sigma}$, corresponding to the parameter i_o is then given by

$$(\Delta i_o)_{1\sigma} = 1/A. \tag{31}$$

This assumes that around the minimum, $\chi^2_t(i_o)$ is a parabola, however, for large variations of i_o, the parabola approximation

is not valid and a better determination of the 1σ error bar can be obtained using the definition

$$(\Delta i_o)_{1\sigma} = |i_o(\chi^2_{min} + 1) - i_o(\chi^2_{min})| \,, \quad (32)$$

which provides two values $(\Delta i_o)_{1\sigma+}$ and $(\Delta i_o)_{1\sigma-}$ (see Lampton et al. 1976; Hébrard et al. 2002).

Because we calculated $\chi^2_t(i_o)$ by minimizing $\chi^2_t(\lambda)$ at each step and for each free parameter λ, we can deduce the range of values corresponding to 1σ for each parameter when the inclination varies between $i_o = i_{o,min} - (\Delta i_o)_{1\sigma-}$ and $i_o = i_{o,min} + (\Delta i_o)_{1\sigma+}$.

Finally, when the best solution corresponding to $M_1 = M_2$ is obtained, we can determine the family of BBH systems with $M_1 \neq M_2$ that provides the same fit.

One important point is that using this phenomenological method, we do not have the proof that the minimum found is unique, since for a completely different set of values for the parameters of the problem, another minimum could exist. However, as we will explore a wide range of inclination angles, i.e. $1^\circ \leq i_o \leq 25^\circ$ and a equally wide range of BBH system masses, i.e. $10^6\ M_\odot \leq M \leq 10^{11}\ M_\odot$, we minimize the possibility of missing the best solution. Another way to overcome this difficulty is to explore the space of possible values of the parameters using, for instance, a Monte Carlo Markov chain algorithm (MCMC algorithm). However this is out of the scope of this article.

4. Application to S5 1803+784

4.1. The radio morphology of S5 1803+784

The blazar S5 1803+784 ($z \approx 0.68$, Lawrence et al. 1987; Stickel et al. 1993) is an intraday-variable (IDV) source with rapid flux-density variations in the optical and radio regime (Wagner & Witzel 1995) on timescales as short as 50 min in the optical (Wagner et al. 1990). The source has been observed and studied with different VLBI arrays at a wide range of frequencies (e.g., Eckart et al. 1986, 1987; Witzel et al. 1988; Charlot 1990; Strom & Biermann 1991; Fey et al. 1996; Gabuzda 1999; Gabuzda & Cawthorne 2000; Gabuzda & Chernetskii 2003; Ros et al. 2000, 2001; Britzen et al. 2005a,b). Global VLBI observations reveal the pc-scale jet of S5 1803+784 to be oriented in the East-West direction (e.g., Britzen et al. 2005b), while the large-scale structure comprises a dominant core component and a weak secondary component ~45″ away from the core at position angle $\Theta \approx -166^\circ$ south-south-west (Antonucci et al. 1986; Britzen et al. 2005a) and makes this source a "misaligned" object (e.g., Pearson & Readhead 1988). Strom & Biermann (1991) also detected this secondary component, as well as a bridge connecting it with the core, at 1.5 GHz observations with the Westerbork Synthesis Radio Telescope (WSRT). World-array VLBI observations revealed that the jet bends by around 90° at a core separation of about 0.5 arcsec towards the South (Britzen et al. 2005a). The Westerbork Synthesis Radio Telescope (WSRT) observations resolved the bridge connecting the core with the secondary component some 45″ to the south. Wiggles in the ridge of this emission suggest that, as on the 100-pc scale, the jet may also oscillate on 50−100 kpc scales. In addition, amorphous emission to the north, as well as an extended, halo-like component around the nucleus has been detected (Britzen et al. 2005a).

On pc-scales the source shows a pronounced jet, with prominent jet components located at distances between 1.4 and 12 mas from the core (e.g., Eckart et al. 1986). Geodetic and astronomical VLBI data obtained at various epochs between 1979 and 1985 indicated that the component at 1.4 mas is stationary (e.g., Schalinski et al. 1988; Witzel et al. 1988). Britzen et al. (2005b) discuss significant position shifts for the 1.4 mas component with displacements between $r \sim 0.7$ mas and $r \sim 1.5$ mas. Obviously the improved time sampling of the geodetic VLBI data led to the detection of systematic position variations for this component regarded as stationary on the basis of the less frequently targeted astronomical observations. This oscillatory behaviour is explained as the result of a reconfinement shock (Britzen et al. 2005b). A recent analysis of 94 epochs of VLBI observations obtained at $\nu = 1.6$, 2.3, 5, 8 15, and 43 GHz reveals that that the jet structure within 12 mas from the core can most easily be described by four jet components that remain at similar core separations in addition to the already known "oscillating" jet feature at ~1.4 mas. We show the pc-scale structure of 1803+784 in an image obtained in VLBA observations performed at 15 GHz (April 2004) in Fig. 2. The jet components are indicated. In addition to these "stationary" components, we find one much fainter component, B3, moving with apparent superluminal velocities. This component most likely coincides with the component seen in 43 GHz maps by Jorstad et al. (2005). However, at 15 GHz this component is much fainter compared to the other components.

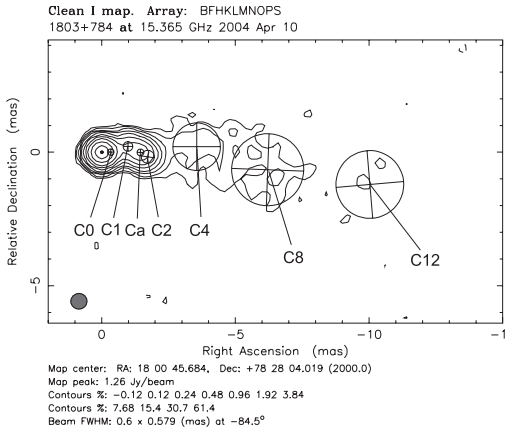

Fig. 2. The pc-scale structure of 1803+784 as obtained in 15 GHz VLBA observations in April 2004. The jet components up to a core separation of ~12 mas are marked.

Evidence is presented for quasi-periodicities in the variability of the core separation, the position angle and the flux of the "oscillating" jet components on timescales comparable to those derived from the total flux density changes (Britzen et al., in prep.; Kudryavtseva et al., in prep.). Superluminal motion has been detected in the jet of S5 1803+784 at 43, 22 (Krichbaum et al. 1993) and 8.4 GHz (Britzen et al. 2005b; Britzen et al., in prep.). In Britzen et al. (2005b) we find and discuss that three jet components approach the brightest and so-called "stationary" component (at ~1.4 mas at 8.4 GHz) with an apparent superluminal motion of 8−11 c. In this paper we show that the "stationary" component oscillates, – under the assumption that this is the brightest jet component in each epoch – and we discuss several possible explanations. Based on the most recently performed investigations of a much larger database (94 epochs of VLBI observations) covering a longer time span (of almost 20 years) and several frequencies (1.6, 2.3, 5, 8.4, and 15 GHz) Britzen et al. find that the brightest jet components near the core do not reveal fast radial motion. Instead, components tend to remain at similar core separations but show significant motion with regard to the position angle. Some indication of apparent superluminal motion between ~5 c and 7 c for the 25 mas jet component

has been derived from 6 and 18 cm observations (Britzen et al. 2005a). VLBI observations at 43 GHz revealed, for the first time, evidence for a jet structure described as "helical" by Krichbaum (e.g., 1990). A curved-jet morphology is found at all scales investigated so far (e.g., Britzen et al. 2005a).

4.2. The observations

For the present analysis we use the archival VLBI observations at two frequencies, 8 and 15 GHz, spanning almost 20 years of observations (for details see Britzen et al., in prep.). S5 1803+784 has been observed with VLBI at $\lambda = 15$ GHz by Pérez-Torres et al. (2000), Kellermann et al. (1998, 2004), and Zensus et al. (2002) between 1994.67 and 2005.68 in 13 epochs. The 8 GHz observations were performed by Ros et al. (2000, 2001) and Pérez-Torres et al. (2000) from 1986.21 to 1993.95 in 41 epochs. The data had been fringe-fitted and calibrated before by the individual observers (for details, see the references given in Britzen et al., in prep.). We performed modelfitting of circular Gaussian components within the *Difmap* package. In order to find the optimum set of components and parameters, we fitted each data set starting from a point-like model. Circular components have been chosen in order to simplify the comparison and to avoid unlikely and extremely extended elliptical components. For details of the data reduction and the modelfit parameters see to Britzen et al. (in prep.).

4.3. Preliminary remarks on the fit

Before we begin the fit of VLBI components of S5 1803+784, we indicate some values we will use for the cosmological parameters and the error bars.

The cosmological model we will use is defined by $\Omega_t = \Omega_\Lambda + \Omega_m$, with $\Omega_\Lambda = 0.7$, $\Omega_m = 0.3$ and $H_0 = 71\ \mathrm{km\,s^{-1}\,Mpc^{-1}}$ for the Hubble constant. Ω_t, Ω_Λ and Ω_m are respectively the total density of the Universe, the density of the vacuum and the density of the matter. Calling z_s the redshift of the source, the luminosity distance, D_l, is defined by

$$D_l = \frac{1+z_s}{H_0}\, c \int_0^{z_s} \frac{\mathrm{d}z'}{E(z')}, \tag{33}$$

where

$$E(z_s) = \sqrt{0.3(1+z_s)^3 + 0.7(1+z_s)}. \tag{34}$$

With $z_s \approx 0.68$ we have $D_l \approx c \times 0.8995/H_0$ and the angular distance is $D_a = D_l/(1+z)^2$.

The beams corresponding to 8 GHz and 15 GHz observations are respectively ≈1.0 mas and ≈0.5 mas. The minimum error bars we will use are $\Delta w = 0.08$ mas and $\Delta n = 0.08$ mas for the West and North coordinates at 8 GHz and $\Delta w = 0.04$ mas and $\Delta n = 0.04$ mas for the West and North coordinates at 15 GHz.

4.4. VLBI components C0, C1 and the trajectory of the ejected plasma component

The jet of S5 1803+784 consists of five "oscillating" jet components, C0 at ∼0.3 mas, C1 at ∼0.7 mas, Ca at ∼1.4 mas, C2 at ∼2 mas and C4 at about ∼4 mas (for the details see Britzen et al. in prep.). In this paper we will discuss only the motion of the two innermost components C0 and C1. Previous analysis has shown that the brightest component Ca, which is quasi-stationary and has almost the same core separation, is changing its position very slowly with a speed of about 0.04 mas/yr (see Fig. 3). This could mean that all the oscillating jet components of S5 1803+784 are moving extremely slowly outwards with time. The pertubation propagation speed of the magnetic tube (the red curve of Fig. 6) is $V_a \ll c$ and is the same for the magnetic loops corresponding to C0, C1 and CA. The source S5 1803+784 has been observed over a time span of 20 years. Thus, we can trace this slow motion of the components with time. The distance from the core of the component C0 is ∼0.3 mas and given a speed of about 0.04 mas/yr it will change its position by ∼0.7 mas in 10 years, which is actually the position of the component C1. Therefore, we can assume that the component C0, which is observed as C0 during the first six years of observations, (between 1986 and 1992), becomes component C1 and from epoch 1996.38 follows the trajectory of this component. So, by using the 20 years of VLBI observations of S5 1803+784 as follows:

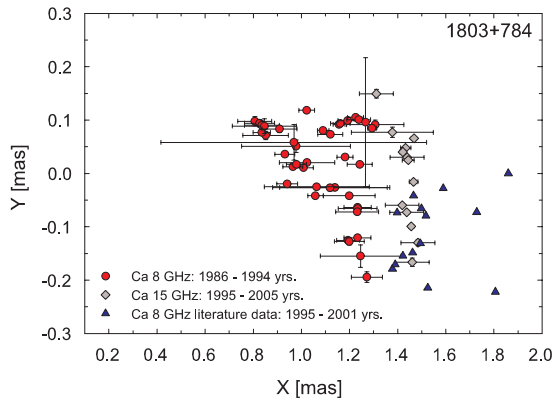

Fig. 3. The movement of the Ca component. The red circles represent the position in rectangular coordinates of the Ca component at 8 GHz during the period 1986−1994. The blue triangles show the position at 8 GHz during 1995−2001 and the grey diamonds the position at 15 GHz from 1995 to 2005. The component moved 0.4 mas during ten years of observations.

1. from 1986.21 to 1991.94, VLBI data corresponding to C0 (8 GHz),
2. for 1993.95, the VLBI point located between C0 and C1 (8 GHz), and
3. from 1996.38 to 2005.68, VLBI data corresponding to C1 (15 GHz),

we can calculate the trajectory that this new plasma component follows and define the moment of ejection from the core, which we find to be around epoch 1984.5 (see the Figs. 4–6). Since there have not been any detected frequency-dependent effects in the position of the jet components (Britzen et al. in prep.), we used 8 and 15 GHz data together for the derivation of the trajectories of the jet components C0 and C1.

Around 1993, 9 years after the ejection of the previous plasma component, a new plasma component arises and follows the magnetic tube in the beam, producing a new VLBI component corresponding to C0 again (see Fig. 2). In fact, the *quasi-stationary component* C0 from Britzen et al. (in prep.) corresponds to the quasi-stationary perturbation of the magnetic tube in which the relativistic plasma propagates. The magnetic tube deformation propagates with a speed $V_a \ll c$.

The existence of a quasi-stationary VLBI component, which seems to be oscillating, can be explained by the fact that firstly the magnetic perturbation of the beam (magnetic loop) is mostly perpendicular to the ejection direction (see Fig. 6) and secondly the observed time between two ejections of the plasma

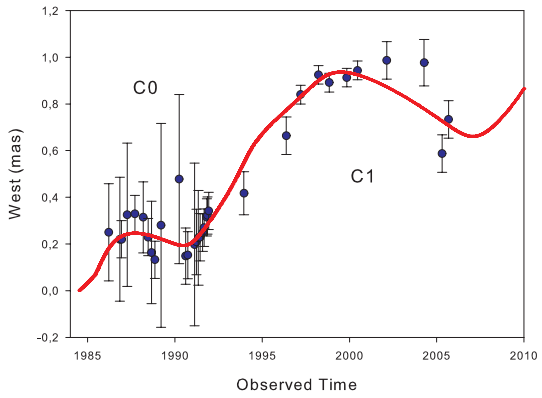

Fig. 4. The West coordinate of $S\,5\ 1803+784$. The smallest error bars for 8 GHz observations are 0.08 mas and for 15 GHz observations are 0.04 mas.

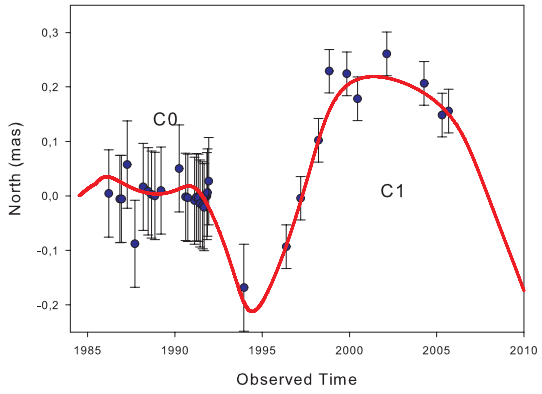

Fig. 5. The North coordinate of $S\,5\ 1803+784$. The smallest error bars for 8 GHz observations are 0.08 mas and for 15 GHz observations are 0.04 mas.

component from the nucleus corresponds to the time for a plasma component to cross the abovementioned magnetic loop.

As the ejection direction is west, the magnetic tube deformation propagating with the speed $V_a \ll c$ will produce a slow motion in the west direction. Moreover, VLBI observations of all the components show a slow bending to the south after the C0 and C1 components. This slow bending can be an effect of the slow motion of the BBH system around the gravity center of the galaxy.

For the VLBI component Ca at ~1.4 mas, which is situated just after C1 (see Fig. 2) slow motion in the south-west direction has been detected over the 20 years of observations. The fit of the model to the trajectories of C0 and C1 predicts that this component will be observed at the present position of Ca and it will move slowly outwards (see Fig. 6). This slow motion is due to both the slow motion of the magnetic perturbation and of the BBH system around the gravity center of the galaxy.

Since the information on the absolute position of the core is lost in interferometric observations, we are not able to determine whether the core is stationary or is itself moving. We will investigate the stationarity of the core in phase reference observations.

As indicated in the introduction, the VLBI core will move due to:

- the motion of the black hole ejecting the VLBI component around the gravity center of the BBH system; and
- the motion of the BBH system around the gravity center of the galaxy.

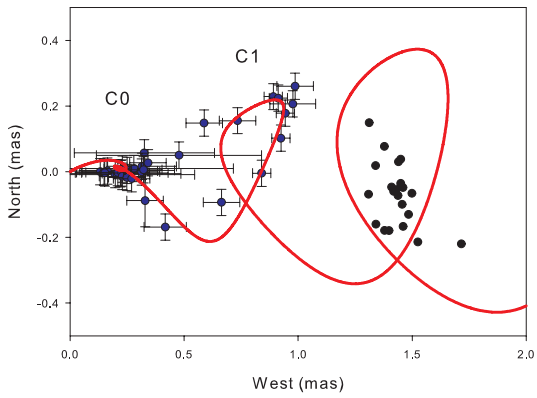

Fig. 6. The trajectory of $S\,5\ 1803+784$. In addition to components C0 and C1, we plotted the points corresponding to the 20 years of observations of the component Ca. The solid line shows the fit of a model to the trajectories of C0 and C1 components. The position of the Ca component lies on the fitted trajectory. This shows the slow motion of the beam perturbation which is due to the perturbation speed $V_a \ll c$ and the slow motion of the BBH system around the gravity center of the galaxy.

4.5. Determination of the minimum of $\chi^2(i_o)$

We first assume $M_1 = M_2$, i.e. that the 2 masses of the BBH system are equal.

From the shape of the trajectory, we find that the precession is defined by $-\omega_p(t - z/V_a)$, thus the orbital rotation has to be $\omega_b(t - z/V_a)$.

As indicated previously, to find the minimum of $\chi^2(i_o)$, we minimize $\chi^2_t(i_o)$ as the inclination angle varies gradually between two values. At each step of i_o, we determine each free parameter λ such that $\chi^2_t(\lambda)$ is minimal for λ.

To determine the trajectory, we integrate (19) using a step Δt. By calling σ_c the size of the ejected component, the parameter n_{rad}, describing the length of the VLBI component along the beam, can be related to σ_c as follows

$$\sigma_c = n_{rad}\ \sin(i_o)\ c\ \Delta t/(D_a \mathrm{mas}). \tag{35}$$

As the inclination varies, we change the integration step in order to keep $\sigma_c = Cst$ if $n_{rad} = Cst$.

As the 2 components C0 and C1 are within 1 mas and the trajectory is complicated, the direction of the ejection, i.e. the parameter $\Delta\Xi$, and the damping time, T_d, of the beam perturbations cannot be properly constrained by the fit of the C0 and C1 coordinates. To find the solution

- the parameter $\Delta\Xi$ is maintained constant, i.e. $\Delta\Xi = 271°$,
- the parameter T_d is kept as a free parameter but with a maximal value $T_d \le T_{d,max} = 1000$ yrs[1].

We calculated $\chi^2_t(i_o)$ when the inclination angle varies between 1° and 25°. The result is shown in Fig. 7.

The inclination angle corresponding to the minimum is $i_o \approx 5.8°$ and the determination of the 1σ using (32) provides $(\Delta i_o)_{1\sigma-} \approx 1.8$ and $(\Delta i_o)_{1\sigma+} \approx 1.7$. Thus we have

$$i_o = 5.8^{+1.7}_{-1.8}. \tag{36}$$

As we calculated the variations of i_o step by step minimizing χ^2 for each variable at each step, we can deduce the range of values corresponding to 1σ for each parameter when the inclination varies between $i_o = i_{o,min} - (\Delta i_o)_{1\sigma-}$ and $i_o = i_{o,min} + (\Delta i_o)_{1\sigma+}$.

[1] The value $T_{d,max} = 1000$ yrs has been chosen to limit the expansion of the perturbation after the third VLBI component and values $T_d \ge T_{d,max}$ do not significantly change the value of χ^2.

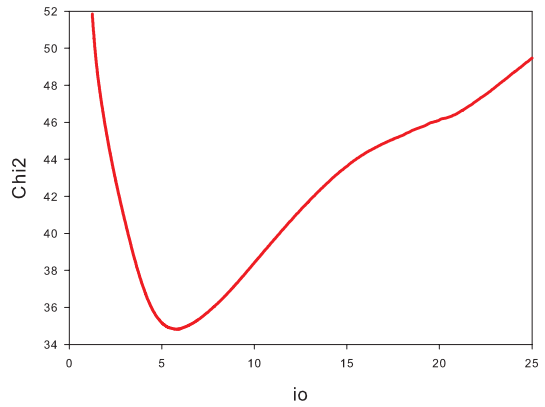

Fig. 7. The variations of $\chi^2_t(i_o)$. There is only one minimum in this interval and it is located at $i_o \approx 5.8°$. The fit has been made using 66 points. As the model uses 12 free parameters the solution is well constrained, as shown by the variations of the curve $\chi^2(i_o)$.

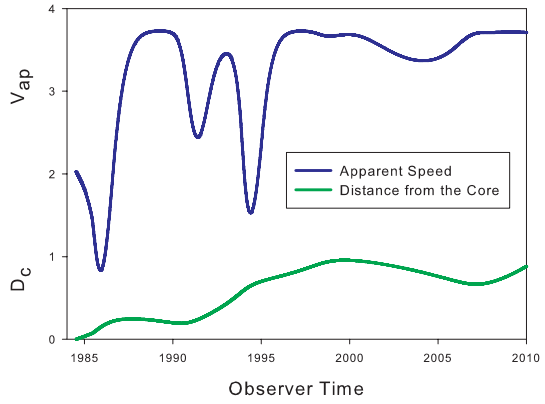

Fig. 8. The variations with time of the apparent speed and the distance from the core of the ejected component. We see that the distance from the core can be mostly constant during certain periods of time. During these periods, the apparent speed is high.

The bulk Lorentz factor of the VLBI component producing C0 and C1 is

$$\gamma_c = 3.7^{+0.3}_{-0.2}. \quad (37)$$

The variations of the apparent speed and the variations of the distance from the core of the VLBI component are shown in Fig. 8. During the times when the motion of the component is mainly perpendicular to the mean ejection direction, as the component moves within a loop of the perturbated magnetic tube, its distance from the core is mostly constant but its apparent speed is high, i.e. $v_{ap} \approx 3.7 \times c$. The periods of time corresponding to these phases are between 1987 and 1990 for the first one and around 2000 for the second one.

We will discuss the results of the BBH system parameters in the next section. However, here we point out an important characteristic of the fit of 1807+784. The better fits are obtained when the ratio T_p/T_b has values close to 1, 2 or 3. The corresponding values of χ^2_{min} are given in Table 1.

From Table 1, we see that the best fit is obtained when $T_p/T_b \approx 2.0$. The results presented in this article correspond to this case.

In Table 2, we give the values of the geometric parameters characterizing the trajectory of the VLBI component producing C0 and C1.

The parameter R_o is found to be $R_o \gg 1$, which indicates that the increase of the perturbation due to the precession is in the linear regime, i.e. $R_o \propto z$ (see Eq. (7)). In that case, χ^2 becomes mostly independent of R_o.

Table 1. Values of χ^2_{min} for different ratios T_p/T_b.

T_p/T_b	χ^2_{min}
≈1	47.1
≈2	34.8
≈3	37.6

Table 2. Geometric parameters of the fit of C0 and C1 for $i_o \approx 5.8$.

Parameter	Value	Unit	Remark
$\Delta\Xi$	271	°	Fixed
Ω	$1.09^{+0.22}_{-0.24}$	°	
R_o	581^{+0}_{-0}	pc	
T_d	1000	yr	$T_{d,max}$
t_o	$1984.51^{+0.32}_{-0.75}$	yr	
n_{rad}	165^{+24}_{-46}	Steps	
$(\tau_{ejec})_{obs}$	$0.96^{+0.33}_{-0.34}$	yr	Obs Frame

Table 3. Families of solutions with $T_p/T_b \approx 2.0$ for $i_o \approx 5.8$.

Family	$\chi^2_t(M_1)$	T_p/T_b
$S1$	≈34.8	1.967
$S2$	≈35.8	2.01

The parameter T_d reaches the maximum allowed value.

The ejection duration of the plasma responsible for the VLBI component in the BBH system frame is

$$(\tau_{ejec})_{bbh} = n_{rad}\,\Delta t \approx 14.47 \text{ yr}, \quad (38)$$

where Δt is the integration step. Note that it does not depend on the observing frequency.

We give in Table 2 the value of the duration of the ejection of the VLBI component in the observer frame. As the time compression factor due to the relativistic ejection defined by t_{obs}/t (see Eq. (26)) is ≈0.0668, the duration of the ejection of the VLBI component in the observer frame is $(\tau_{ejec})_{obs} \approx 0.96$ yr.

The parameter n_{rad} also characterizes the length of the VLBI component along the beam. This length is $\sigma_c \approx 0.07$ mas.

The fit has been mqde using 66 points (33 points for each coordinate). As the model uses 12 free parameters (indeed $\Delta\Xi = Cst$ and $T_d = T_{d,max} = \text{const.}$), the solution is well constrained as shown by Fig. 7.

4.6. Determination of the family of BBH systems

Starting from the solution found in Sect. 4.5, we fix the parameters $i_o = i_{o,min}$, $t_o = 1984.51$, $n_{rad} = 165$ and we study the variations of χ^2 when the mass M_1 varies between $10^6\ M_\odot$ and $10^{11}\ M_\odot$ (with the assumption $M_1 = M_2$ still holding true).

This allows us to find whether, for a given mass, unique solutions, or families of solutions exit. For the latter case, we find that $\chi^2_t \approx Cst$ when the parameter M_1 varies, i.e. the parameter M_1 shows a degeneration.

We find that there are 2 families corresponding to the ratio $T_p/T_b \approx 2.0$. The results corresponding to these families are given in Table 3.

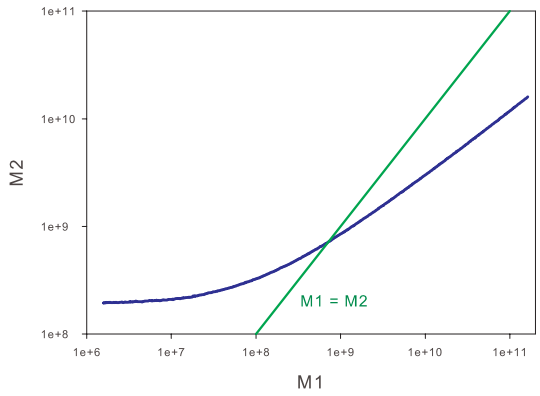

Fig. 9. The family of possible BBH systems with $M_1 \neq M_2$ corresponding to the solution $S\,1c$ of Table 4 from Appendix B.

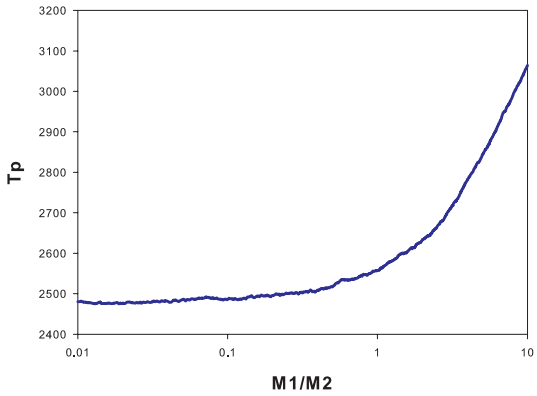

Fig. 10. The precession period as a function of the ratio M_1/M_2.

The best fit corresponds to the family $S\,1$ for which we have

$$\frac{T_\mathrm{p}}{T_\mathrm{b}} \approx 1.967. \tag{39}$$

To find the relations between the parameters of the family, we determined the parameters for 4 different values of the mass M_1. The results are given in Table 4 of Appendix B.

For all the *members* of the family, the parameters of Table 2 are the same and the parameters ϕ_o and ψ_o are also the same. Only the parameters T_p, T_b and V_a change when the mass changes. Moreover, they are correlated and in Table 4 (Appendix B), the relations between them are given.

The precession period is proportional to the inverse of the square root of the mass M_1, i.e.

$$T_\mathrm{p} \propto M_1^{-1/2}, \tag{40}$$

the ratio $T_\mathrm{p}/T_\mathrm{b}$ is the same for all the members of the family, so

$$T_\mathrm{p} \approx 1.967\ T_\mathrm{b}, \tag{41}$$

and the Alfven speed is mostly proportional to the inverse of the precession period, i.e.

$$V_\mathrm{a} \propto 1/T_\mathrm{p}^{0.954} \propto M_1^{0.477}. \tag{42}$$

Thus, if the parameters of a member of the family are known, we can deduce the parameters for the rest of the members of the family, as M_1 varies.

From VLBI observations alone, we cannot determine the mass of the BBH system in the nucleus of S5 1803+784. However from the knowledge of the family of solutions, we can illustrate the characteristics of the BBH system assuming a range of masses corresponding, for instance, to the range between the solutions $S\,1c$ and $S\,1d$, i.e. $7.14 \times 10^8 \leq M_1 \leq 5.92 \times 10^9\ M_\odot$. We find that the precession period is $2557.5 \geq T_\mathrm{p} \geq 892.0$ yr and the orbiting period is $1299.7 \geq T_\mathrm{b} \geq 453.2$ yr.

When $M_1 = M_2$, the size of the BBH system is the same for all the members of the family and is 0.100 mas.

4.7. The families of solutions with $M_1 \neq M_2$

In the previous sections we looked for solutions assuming $M_1 = M_2$.

However, it is possible to find solutions with $M_1 \neq M_2$, starting from the solutions found previously. To illustrate this possibility, we start from the solution $S\,1c$ of the previous section (see Appendix B) and find the family of solutions with $M_1 \neq M_2$ which produces the same fit.

Assuming $i_\mathrm{o} = 5.8°$, $t_\mathrm{o} = 1984.51$ and $n_\mathrm{rad} = 165$, we gradually vary the mass M_1 between $1.5{\times}10^6$ and $1.6{\times}10^{11}$ and we determine M_2 minimizing χ^2 for each free parameter at each step. The corresponding range of M_2 is $1.9 \times 10^8 \leq M_2 \leq 1.6 \times 10^{10}$ and the corresponding ratio M_1/M_2 is $0.01 \leq M_1/M_2 \leq 10$.

The family has been plotted in Fig. 9.

The precession period corresponding to different ratios M_1/M_2 has been plotted in Fig. 10.

For all the *members* of the family solution $S\,1c$ with $M_1 \neq M_2$, all the parameters of Table 2 are the same and the parameters ϕ_o and ψ_o are also the same. Only the parameters T_p, T_b and V_a change when the ratio M_1/M_2 changes.

The changes of the parameters T_p, T_b and V_a are characterized by

1. when $M_1 \to 0$, $M_2 \to 1.98 \times 10^8\ M_\odot$;
2. when $M_1 \ll M_2$, $T_\mathrm{p} \approx Cst \approx 2480$ yr;
3. when $M_1 \gg M_2$, T_p increases proportionaly with M_1/M_2;
4. $T_\mathrm{p} \approx 1.967\ T_\mathrm{b}$;
5. the Alfven speed V_a is mostly proportional to the inverse of T_p, i.e.

$$V_\mathrm{a} \propto 1/T_\mathrm{p}^{0.958}; \tag{43}$$

6. the size of the BBH system varies from $R_\mathrm{bbh} \approx 0.050$ mas when $M_1/M_2 \to 0$ to $R_\mathrm{bbh} \approx 0.558$ mas when $M_1/M_2 = 10$ see Fig. 11.

Therefore, the main difference between the variations of the parameters T_p, T_b and V_a for families with $M_1 = M_2$ and $M_1 \neq M_2$ concerns the relation between T_p and M_1. When $M_1 = M_2$, we have $T_\mathrm{p} \propto M_1^{-1/2}$ and when $M_1 \neq M_2$ the variations between T_p and M_1/M_2 are shown in Fig. 10.

5. Discussion and conclusion

Assuming that the nucleus of a radio source contains a BBH system, we presented a new method to fit the variations of both coordinates of a VLBI component as a function of time. This method is self consistent and solves the problems of the previous method, the two step method, used in Lobanov & Roland (2005). The presence of a BBH system produces two perturbations of the magnetic tube in which the plasma, that is responsible for the radio emission of the VLBI component, propagates. These two perturbations are due to the precession of the accretion disk and the motion of the black holes around the gravity center of

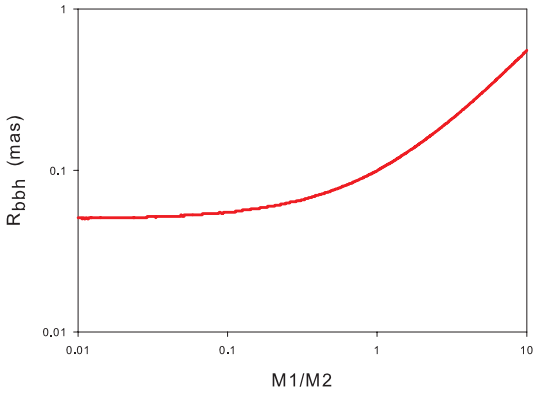

Fig. 11. The size of the BBH system as a function of the ratio M_1/M_2.

the BBH system. The model is a geometric model and as we fit only the VLBI coodinates, the problem reduces to an astrometric problem. As the knowledge of the variations of the coordinates contains kinematical information, we are able to deduce the inclination angle of the source and the bulk Lorentz factor of the ejected VLBI component. The fit must be done following the trajectory of one VLBI component and not using data of several components. Indeed, as a VLBI component follows the perturbed magnetic tube, two VLBI components will not follow exactly the same trajectories because the magnetic field perturbation propagates. In addition to the two perturbations due to the BBH system, we can have a third one due to the slow motion of the BBH system around the gravity center of the galaxy. This third perturbation can be responsible for the slow bending of the VLBI jet that is often observed in compact radio sources. When it is observed, it is generally at a distance from the core larger than a few mas. Then studying the motion of the VLBI component in the first mas, we can expect that the influence of the slow motion of the BBH system around the galactic gravity center is negligible compared to the perturbations due to the precession of the accretion disk and the motion of the black holes around the gravity center of the BBH system. So to obtain the characteristics of the BBH system in the nucleus of the radio galaxy, we have to fit the data concerning the VLBI component within 1 or 2 mas only.

To illustrate the method, we applied it to 1803+784 for which we have 20 years of observations. This allows us to follow the VLBI component as it propagates through the two first perturbations of the magnetic tube. These perturbations correspond to C0 and C1, which have been called oscillatory VLBI components by observers.

Assuming, at first, that the two black holes have the same mass, we find for 1803+784 that

1. the inclination of the source is $i_o = 5.8^{+1.7}_{-1.8}$;
2. the bulk Lorentz factor of the ejected component is $\gamma_c = 3.7^{+0.3}_{-0.2}$;
3. the angle between the accretion disk and the plane of the BBH system is $\Omega = 1.09^{+0.22}_{-0.24}$;
4. the size of the BBH system is ≈0.100 mas;
5. the precession period of the accretion disk, T_p, and the orbiting period of the BBH system, T_b, are related by $T_p \approx 1.967\ T_b$;
6. the origin of the component is $t_o = 1984.51^{+0.32}_{-0.75}$;
7. the duration of the ejection of the plasma responsible for the VLBI component is $(\tau_{ejec})_{obs} = 0.93^{+0.33}_{-0.34}$ yr in the observer frame which corresponds to $(\tau_{ejec})_{bbh} \approx 13.9$ yr in the BBH frame.

We find that there is not a unique solution for the mass of the BBH system, but a family of solutions that produces the same fit. For all the *members* of the family, all the parameters are the same, except the parameters T_p, T_b and V_a which change when the mass changes. The variation laws for these parameters are:

$$T_p \propto M_1^{-1/2}, \tag{44}$$

$$V_a \propto 1/T_p^{0.954} \propto M_1^{0.477}, \tag{45}$$

the ratio T_p/T_b is the same for all the members of the family, so

$$T_p \approx 1.967\ T_b. \tag{46}$$

Thus, if the parameters of a member of the familly are calculated, we can subsequently deduce the parameters of all the members of the family when M_1 varies.

To illustrate the characteristics of the BBH system, if we assume a range of masses corresponding to $7.14\ 10^8\ M_\odot \le M_1 \le 5.92\ 10^9\ M_\odot$, we find that the precession period is 2557.5 yr ≥ T_p ≥ 892.0 yr, the orbit period is 1299.7 yr ≥ T_b ≥ 453.2 yr .

Furthermore, from the knowledge of the solution with $M_1 = M_2$, we can find the families with $M_1 \neq M_2$.

If VLBI observations allow us to find the possible families of BBH system solutions and the main characteristics of these systems, radio sources exist for which, in addition to VLBI data, optical bursts associated with the birth of the VLBI component have been observed (see for instance Britzen et al. 2001, in the case of 0420-014; and Lobanov & Roland 2005, for 3C 345). The combination of VLBI and optical observations can further constrain the families of solutions.

Acknowledgements. N. A. Kudryavtseva and M. Karouzos were supported for this research through a stipend from the International Max Planck Research School (IMPRS) for Radio and Infrared Astronomy at the Universities of Bonn and Cologne. We thank the anonymous referee for carefully reading the manuscript and many valuable comments.

Appendix A: Coefficients *A*, *B* and *C*

Let us call

$$\phi(t) = \omega_p t - k_p z(t) + \phi_o, \tag{47}$$

and

$$\psi(t) = \omega_b t - k_b z(t) + \psi_o. \tag{48}$$

With

$$x_1 = y_1 = -\frac{M_2}{M_1 + M_2}\left[\frac{T_b^2}{4\pi^2} G(M_1 + M_2)\right]^{1/3}, \tag{49}$$

the coefficients A, B and C of Eq. (22) are given by

$$\begin{aligned} A = \exp(-2t/T_d)\Bigg[&\frac{\omega_b \omega_p R(z)}{V_a^2}(y_1 + x_1)\cos(\psi(t) - \phi(t)) \\ &+ \frac{\omega_b}{V_a}\frac{dR}{dz}(x_1 + y_1)\sin(\psi(t) - \phi(t)) + \frac{\omega_p^2 R(z)^2}{V_a^2} \\ &+ \left(\frac{dR}{dz}\right)^2 + \frac{\omega_b^2}{2V_a^2}(x_1^2 + y_1^2)\Bigg] + 1. \end{aligned} \tag{50}$$

$$
\begin{aligned}
B \;=\; & \exp(-2t/T_{\rm d})\left[\frac{2x_1\omega_{\rm b}x_1\cos(\psi_{\rm o})}{T_{\rm d}V_{\rm a}}\sin(\psi(t))\right.\\
& -\frac{2y_1\omega_{\rm b}y_1\sin(\psi_{\rm o})}{T_{\rm d}V_{\rm a}}\cos(\psi(t))\\
& +2\left(\frac{{\rm d}R(z)}{{\rm d}z}x_1\cos(\psi_{\rm o})-\frac{y_1\sin(\psi_{\rm o})R(z)\omega_{\rm p}}{V_{\rm a}}\right)\cos(\phi(t))\\
& +2\left(\frac{{\rm d}R(z)}{{\rm d}z}y_1\sin(\psi_{\rm o})+\frac{x_1\cos(\psi_{\rm o})R(z)\omega_{\rm p}}{V_{\rm a}}\right)\sin(\phi(t))\\
& +\sin(\psi(t)-\phi(t))\left\{-\omega_{\rm b}\frac{{\rm d}R(z)}{{\rm d}z}(x_1+y_1)\right.\\
& \left.+\frac{(\omega_{\rm p}-\omega_{\rm b})R(z)}{V_{\rm a}}(x_1+y_1)/T_{\rm d}\right\}\\
& +\cos(\psi(t)-\phi(t))\left\{-\frac{2\omega_{\rm p}\omega_{\rm b}R(z)}{V_{\rm a}}(x_1+y_1)\right.\\
& \left.-\frac{{\rm d}R(z)}{{\rm d}z}(x_1+y_1)/T_{\rm d}\right\}-\frac{\omega_{\rm b}^2}{V_{\rm a}}\left(x_1^2+y_1^2\right)\\
& \left.-\frac{2\omega_{\rm p}^2R^2(z)}{V_{\rm a}}-\frac{2{\rm d}R(z)}{{\rm d}z}\frac{R(z)}{T_{\rm d}}\right]. \qquad (51)
\end{aligned}
$$

$$
\begin{aligned}
C \;=\; & \exp(-2t/T_{\rm d})\left[\frac{(x_1\cos(\psi_{\rm o}))^2+(y_1\sin(\psi_{\rm o}))^2}{T_{\rm d}^2}\right.\\
& +2\left(\frac{y_1\omega_{\rm b}y_1\sin(\psi_{\rm o})}{T_{\rm d}}-\frac{x_1x_1\cos(\psi_{\rm o})}{T_{\rm d}^2}\right)\cos(\psi(t))\\
& -2\left(\frac{x_1\omega_{\rm b}x_1\cos(\psi_{\rm o})}{T_{\rm d}}-\frac{y_1y_1\sin(\psi_{\rm o})}{T_{\rm d}^2}\right)\sin(\psi(t))\\
& +2R(z)\left(\frac{y_1\sin(\psi_{\rm o})\omega_{\rm p}}{T_{\rm d}}-\frac{x_1\cos(\psi_{\rm o})}{T_{\rm d}^2}\right)\cos(\phi(t))\\
& -2R(z)\left(\frac{x_1\cos(\psi_{\rm o})\omega_{\rm p}}{T_{\rm d}}+\frac{y_1\sin(\psi_{\rm o})}{T_{\rm d}^2}\right)\sin(\phi(t))\\
& +\sin(\psi(t)-\phi(t))\left\{-(\omega_{\rm b}-\omega_{\rm p})R(z)(x_1+y_1)/T_{\rm d}\right\}\\
& +\cos(\psi(t)-\phi(t))\left\{\omega_{\rm p}\omega_{\rm b}R(z)(x_1+y_1)\right.\\
& \left.-R(z)(x_1+y_1)/T_{\rm d}^2\right\}+\frac{\omega_{\rm b}^2}{2}\left(x_1^2+y_1^2\right)+R^2(z)\omega_{\rm p}^2\\
& \left.+\left(R^2(z)+\frac{x_1^2+y_1^2}{2}\right)/T_{\rm d}^2\right]-v^2. \qquad (52)
\end{aligned}
$$

Appendix B: BBH parameters for 4 values of M_1 of the family S1

The BBH parameters for 4 values of M_1 of the family S1 are given in Table 4.

Table 4. BBH parameters for 4 values of M_1 of the family S1.

	S 1*a*	*S* 1*b*	*S* 1*c*	*S* 1*d*
$\phi_{\rm o}$	78.9	78.8	79.0	79.1
$T_{\rm p}$	16380.4	6608.55	2557.47	891.95
M_1	1.7556×10^7	1.0743×10^8	7.1437×10^8	5.9232×10^9
$\psi_{\rm o}$	59.5	59.5	59.5	59.8
$T_{\rm b}$	8326.9	3360.29	1299.68	453.198
$V_{\rm a}$	0.0078855	0.019298	0.048358	0.12665

For all the *members* of the family, all the parameters of Table 1 are the same and the parameters $\phi_{\rm o}$ and $\psi_{\rm o}$ are also the same. Only the parameters $T_{\rm p}$, $T_{\rm b}$ and $V_{\rm a}$ change when the mass M_1 changes.

References

Achatz, U., & Schlickeiser, R. 1993, A&A, 274, 165
Antonucci, R. R. J., Hickson, P., Olszewski, E. W., & Miller, J. S. 1986, AJ, 92, 1
Attridge, J. M., Roberts, D. H., & Wardle, J. F. C. 1999, ApJ, 518, 87
Benford, G., & Lesch, H. 1998, MNRAS, 301, 414
Biretta, J. A., Sparks, W. B., & Macchetto, F. 1999, ApJ, 520, 621
Britzen, S., Roland, J., Laskar, J., et al. 2001, A&A, 374, 784
Britzen, S., Krichbaum, T. P., Strom, R. G., et al. 2005a, A&A, 444, 443
Britzen, S., Witzel, A., Krichbaum, T. P., et al. 2005b, MNRAS, 362, 966
Britzen, S., Kudryavtseva, N. A., Witzel, A., et al. 2007, A&A, submitted
Camenzing, M., & Krokenberger, M. 1992, A&A, 255, 59
Charlot, P. 1990, A&A, 229, 51
Eckart, A., Witzel, A., Biermann, P., et al. 1986, A&A, 168, 17
Eckart, A., Witzel, A., & Biermann, P. 1987, A&ASS, 67, 121
Fey, A. L., Clegg, A. W., & Fomalont, E. B. 1996, ApJS, 105, 299
Gabuzda, D. C. 1999, NewAR, 43, 691
Gabuzda, D. C., & Cawthorne, T. V. 2000, MNRAS, 319, 1056
Gabuzda, D. C., & Chernetskii, V. A. 2003, MNRAS, 339, 669
Gomez, J.-L., Marscher, A. P., Alberdi, A., Jorstad, S. G., & Agudo, I. 2001, ApJ, 521, L161
Hébrard, G., Lemoine, M., Vidal-Madjar, A., et al. 2002, ApJS, 140, 103
Jorstad, S. G., Marscher, A. P., Lister, M. L., & Stirling, A. M. 2005, AJ, 130, 1418
Kellermann, K. I., Vermeulen, R. C., & Zensus, J. A. 1998, AJ, 115, 1295
Kellermann, K. I., Lister, M. L., Homan, D. C., et al. 2004, ApJ, 609, 539
Krichbaum, T. P. 1990, in Parsec-scale Radio Jets, ed. J. A. Zensus, & T. J. Pearson (Cambridge: Cambridge University Press), 83
Krichbaum, T. P., Witzel, A., Graham, D. A., et al. 1993, in Subarcsecond Radio Astronomy, ed. R. J. Davies, & R. S. Booth (Cambridge: Cambridge University Press), 181
Kudryavtseva, N .A., Britzen, S., Witzel, A., et al., in prep.
Lampton, M., Margon, B., & Bowyer, S. 1976, 208, 177
Lawrence, C. R., Readhead, A. C. S., Pearson, T. J., & Unwin, S. C. 1987, in Superluminal Radio Sources, ed. J. A. Zensus, & T. J. Pearson (Cambridge: Cambridge University Press), 260
Lobanov, A., & Roland, J. 2005, A&A, 431, 831
Marcowith, A., Henri, G., & Pelletier, G. 1995, MNRAS, 277, 681
Marcowith, A., Henri, G., & Renaud, N. 1998, A&A, 331, L57
Muxlow, T. W. B., Pelletier, G., & Roland, J. 1988, A&A, 206, 237
Pearson, T. J., & Readhead, A. C. S. 1988, ApJ, 328, 114
Pelletier, G., & Roland, J. 1989, A&A, 224, 24
Pelletier, G., & Roland, J. 1990, in Parsec-Scale Jets, ed. J. A. Zensus, & T. J. Pearson (Cambridge: Cambridge University Press), 323
Pelletier, G., & Sol, H. 1992, MNRAS, 254, 635
Pelletier, G., Sol, H., & Asseo, E. 1988, Phys. Rev. A, 38, 2552
Pérez-Torres, M. A., Marcaide, J. M., Guirado, J. C., et al. 2000, A&A, 360, 161
Roland, J., & Hermsen, W. 1995, A&A, 297, L9
Roland, J., & Hetem, A. 1996, in Cygnus A: Study of a radio galaxy, ed. C. L. Carilli, & D. E. Harris (Cambridge: Cambridge University Press), 126
Roland, J., Peletier, G., & Muxlow, T. 1988, A&A, 207, 16
Roland, J., Teyssier, R., & Roos, N. 1994, A&A, 290, 357
Ros, E., Marcaide, J. M., Guirado, J. C., et al. 2000, A&A, 356, 357
Ros, E., Marcaide, J. M., Guirado, J. C., & Pérez-Torres, M. A. 2001, A&A, 376, 1090
Schalinski, C. J., Alef, W., Witzel, A., et al. 1988, in ed. M. J. Reid, & J. M. Moran, Proc. IAU Symp., 129 (Kluwer: Dordrecht), 359
Skibo, J. G., Dermer, C. D., & Schlickeiser, R. 1997, ApJ, 483, 56
Sol, H., Pelletier, G., & Asseo, E. 1989, MNRAS, 237, 411
Stickel, M., Fried, J. W., & Kühr, H. 1993, A&AS, 98, 393
Strom, R. G., & Biermann, F. L. 1991, A&A, 242, 313
Tingay, S. J., Jauncey, D. L., Reynolds, J. E., et al. 1998, AJ, 115, 960
Wagner, S., Sanchez-Pons, F., Quirrenbach, A., & Witzel, A. 1990, A&A, 235, L1
Wagner, S. J., & Witzel, A. 1995, ARA&A, 33, 163
Witzel, A., Schalinski, C. J., Johnston, K. J., et al. 1988, A&A, 206, 245
Zensus, J. A., Ros, E., Kellermann, K. I., et al. 2002, AJ, 124, 662